1   **Title: Sharp 660-km discontinuity controlled by extremely narrow binary post-**

2   **spinel transition**

3

4   **Authors:** Takayuki Ishii[*,1], Rong Huang[1], Robert Myhill[2], Hongzhan Fei[1], Iuliia

5   Koemets[1], Zhaodong Liu[1], Fumiya Maeda[3], Liang Yuan[3], Lin Wang[1], Dmitry Druzhbin[1],

6   Takafumi Yamamoto[4], Shrikant Bhat[1,5], Robert Farla[5], Takaaki Kawazoe[1,4], Noriyoshi

7   Tsujino[6], Eleonora Kulik[1,5], Yuji Higo[7], Yoshinori Tange[7], Tomoo Katsura[1]

8

9   **Affiliations:**

10   [1]Bayerisches Geoinstitut, University of Bayreuth, Universitätsstraße 30, 95440 Bayreuth,

11   Germany

12   [2]School of Earth Sciences, University of Bristol, Wills Memorial Building, Queens Road,

13   Bristol BS8 1RJ, UK

14   [3]Department of Earth Sciences, Graduate School of Science, Tohoku University, 6-3,

15   Aramaki Aza Aoba, Aoba, Sendai, Miyagi 980-8578, Japan

16   [4]Department of Earth and Planetary Systems Science, Graduate School of Science,

17   Hiroshima University, Kagamiyama 1-3-1, Higashi-Hiroshima, 739-8526 Japan

18   [5]Deutsche Elektronen-Synchrotron (DESY), Notkestraße 85, 22607 Hamburg, Germany

19   [6]Institute for Study of the Earth's Interior, Okayama University, Misasa, 682-0193 Japan

20   [7]Japan Synchrotron Radiation Research Institute (JASRI), 1-1-1, Kouto, Sayo-cho, Sayo-

21   gun, Hyogo 679-5198 Japan

22   ***Corresponding author:** Takayuki Ishii (takayuki.ishii@uni-bayreuth.de)

Abstract:

The Earth's mantle is characterised by a sharp seismic discontinuity at a depth of 660-km that can provide insights into deep mantle processes. The discontinuity occurs over only 2km - or a pressure difference of 0.1 GPa - and is thought to result from the post-spinel transition, that is, the decomposition of the mineral ringwoodite to bridgmanite plus ferropericlase. Existing high-pressure-temperature experiments have lacked the pressure control required to test whether such sharpness is the result of isochemical phase relations or chemically distinct upper and lower mantle domains. Here, we obtain the isothermal pressure interval of the Mg-Fe binary post-spinel transition by applying advanced multi-anvil techniques with *in situ* X-ray diffraction with help of Mg-Fe partition experiments. It is demonstrated that the interval at mantle compositions and temperatures is only 0.01 GPa, corresponding to 250 m. This interval is indistinguishable from zero at seismic frequencies. These results can explain the discontinuity sharpness and provide new support for whole mantle convection in a chemically homogeneous mantle. The present work suggests that distribution of adiabatic vertical flows between the upper and lower mantles can be mapped based on discontinuity sharpness.

Main:

The 660-km seismic discontinuity (D660) is the boundary between the upper and lower mantles. Seismological studies based on short-period *P*-wave reflections (*P′660P′-P′P′*) have demonstrated that D660 is extremely sharp and less than 2 km thick[1], which is in striking contrast to the 7-km-thick 410-km discontinuity[1]. Understanding the nature of D660 from a perspective of mineral physics provides important clues to open questions about the structure and dynamic processes in the Earth's mantle, such as slab subduction and upwelling of hot plume.

Geochemical studies suggest that the Earth's upper mantle consists of ca. 60% atom-

proportion of the $(Mg,Fe)_2SiO_4$ polymorphs with Mg/Mg+Fe ratios around 0.9, including olivine (Ol), wadsleyite, and ringwoodite (Rw), with the remaining 40% consisting primarily of ortho- and clinopyroxenes and garnet (Gt). In contrast, the lower mantle consists of ca. 70 atom % $(Mg,Fe)SiO_3$ compounds, such as bridgmanite (Brg) and post-perovskite with ca. 20 atom % ferropericlase (fPc) and 10% calcium perovskite. Because the discontinuity depth is close to the pressure of the post-spinel transition, dissociation of Rw to Brg + ferropericlase (fPc)[2] and the elastic wave velocities of the post-spinel phase are distinctively higher than those of ringwoodite, it is usually considered that the D660 should be caused by the post-spinel transition.

Whether or not the PSp transition can explain D660 constrains the chemical structure of the mantle (homogeneous versus chemically layered mantle)[3,4] and the type of mantle convection (whole-mantle versus layered-mantle convection)[5,6]. If D660 is due to the PSp transition, slabs may be able to be subducted to the lower mantle because of a homogenous mantle across D660, leading to whole-mantle convection. However, if D660 is not due to the transition, a compositionally distinct upper and lower mantle is required to explain D660, which must imply layered-mantle convection (e.g. Refs 7, 8).

If the small thickness of the D660 primarily corresponds to the pressure interval of three-phase coexistence of Rw + Brg + fPc in the Mg-Fe (pseudo)binary PSp transition, this binary loop must be extremely narrow and less than 0.1 GPa in pressure. However, such a narrow binary loop has never been demonstrated by mineral physics data. Reference 2 first attempted to determine the transition interval through a conventional multi-anvil experiment, in which pressures were determined with a precision of ~0.5 GPa. The experiment was based on the spatial dimension of Rw + Brg + fPc coexistence along a temperature gradient obtained by micro-focused X-ray diffractometry and the Clapeyron slope of the PSp transition that they determined. The strategy was invalid, however, because of the limited spatial resolution of laboratory micro-focused X-ray diffractometry and controversial Clapeyron slope of the PSp transition. Reference

9 attempted to determine the interval by precise multi-anvil experiments in combination with *in situ* X-ray diffraction, obtaining a pressure interval of ≤1 GPa. However, they determined pressures with a precision of ~0.2 GPa and observed pressure drop despite constant press load and temperature. The pressure drop may have led to serious overestimation of the pressure interval because the PSp phase remains even in a Rw stability field due to the sluggish reversal reaction[10]. Furthermore, a thermodynamic calculation to depict the precise binary loop was also hampered because thermodynamic data for a hypothetical $FeSiO_3$ endmember of Brg were lacking[11]. An experimental approach with pressure precision better than 0.1 GPa and precisely maintaining a target pressure to eliminate the kinetic problem[10] is essential for examining whether the binary loop is narrow enough to account for the sharp D660.

In this study, we determined the binary loop thickness of the PSp transition in the system Mg_2SiO_4-Fe_2SiO_4, using a combination of a Kawai-type multi-anvil press and *in situ* X-ray diffraction with precise pressure control to overcome the above technical problems. We adopted the following initiatives on pressure control during an experiment (Ref. 12 and see the Methods section for details). Sample pressures with a relative precision of ~0.05 GPa were achieved because of high-quality X-ray diffraction pattern of the MgO pressure marker with many peaks and high counts obtained by our advanced experimental technology[12,13] (Extended Data Figs. 1 and 2). This approach allowed us to determine the difference between the transition pressures at Fo_{100} and Fo_{70} compositions with precisions of 0.1 GPa. The pressure drop at a high temperature[9] was suppressed by increasing press load (the forced-pumping technique[12,13]). It is emphasized that two samples with bulk compositions of Mg_2SiO_4 (Fo_{100}) and $(Mg_{0.7}Fe_{0.3})_2SiO_4$ (Fo_{70}) were loaded in one run to simultaneously determine their transition pressures (Extended Data Figs. 2 and 3). Since the binary loop of Rw + Brg + *f*Pc ends near the Fo_{70} composition according to previous high-pressure experiments and thermodynamic calculation[2,11] because of the stabilization of stishovite (St) + *f*Pc assembly this procedure permits the most precise constraint

of the pressure range of the binary loop (Fig. 1). The starting materials were mixtures of Ol, orthopyroxene, and (*f*)Pc, which allowed both normal and reversal transitions[12]. The width of the binary loop in composition was estimated based on the difference in the transition pressures at Fo_{100} and Fo_{70} compositions and available thermodynamic data from the partitioning experiments[14-17].

Determination of the binary post-spinel transition

The binary phase relations determined at 1700 K are shown in Fig. 1. A striking feature is that the transition pressure in the Fo_{70} composition (between 23.86(6) and 24.00(5) GPa) is higher than that in the Fo_{100} composition (between 23.72(5) and 23.86(6) GPa) by 0.14 GPa, beyond the present uncertainty (0.11 GPa). The higher transition pressure with more Fe-rich composition differs from the consensus regarding the phase relations in this system after Ref. 2. Note that the run at 23.86(6) GPa (M2268) shows that Brg + Pc is stable in a Fo_{100} composition and Rw is stable in a Fo_{70} composition (Fig. 2 and Extended Data Figs. 4b). The geometry of the phase diagram shows that the pressure interval of the binary loop at $(Mg_{0.9}Fe_{0.1})_2SiO_4$ (Fo_{90}) should be much smaller than this pressure difference (0.14 GPa).

The pressure intervals at Fo_{90} were quantitatively estimated at 1700 and 2000 K using compositions of the three phases (Brg, *f*Pc and Rw) between the Mg endmember and the four-phase coexistence boundary calculated with thermodynamic data because it is impossible to reach chemical equilibrium within limited experimental hours in the synchrotron radiation facility due to small diffusion coefficients[20,21] and also because very small grain sizes (less than 3 μm) of recovered phases were too small for compositional analysis by electron microprobe (see the Methods section and Extended Data Table 2 and 3). We calculated compositions of Brg and Rw for a given *f*Pc composition by using the Gibbs energy changes by Mg-Fe exchange between Brg and *f*Pc[15] and between Rw and *f*Pc[16], and interaction parameters of the three phases[15-17]. We changed the *f*Pc composition step by step from the Mg-end member and repeated this calculation

until the Fe content in Brg reaches the maximum solubility reported by Ref. 14. The pressures for these three-phase coexistences were calculated by the phase compositions, their volume at pressures and temperatures of interest, and the interaction parameters to depict the binary loop.

Extremely narrow binary post-spinel transition

The binary loop thus obtained is curved and has very close Mg and Fe contents between Rw and Brg + fPc, which agrees to previous thermodynamic calculations[22,23]. The pressure interval is found 0.012±0.008 GPa at a bulk composition of Fo_{90} at 1700 K as shown in Fig. 1. This interval is by one order of magnitude smaller than the previous estimation (0.15 GPa)[2]. This pressure interval corresponds to a depth interval of only 100–500 m, which is also one order of magnitude smaller than the observable thickness of D660 using 1 Hz seismic waves (less than 2 km)[1]. The pressure interval at an expected mantle temperature, namely, 2000 K[24], was evaluated by the same procedure. The Clapeyron slope reported by Ref. 19 was used and modified using the MgO scale suggested by Ref. 18 to estimate transition pressures at Mg endmember and the 4-phase coexistence. We obtained a pressure interval at 2000 K of 0.003±0.002 GPa, which is even smaller than that at 1700 K.

One consideration is that incorporation of secondary components such as Fe_2O_3, Al_2O_3, and water may change the pressure interval by changing the compositions of Rw and Brg, and by stabilizing Gt. Our thermodynamic calculations show that the pressure interval in more natural compositions will be less than or similar to that in the present Mg-Fe^{2+} binary system. In particular, Gt has the important role of buffering the Fe^{3+} and Al^{3+} contents of Brg, which would otherwise broaden the transition (Supplementary discussion for details). The reducing effect of non-transforming phase such as Gt was also discussed in Ref. 25. Thus, the seismically observed sharpness of D660 is in excellent agreement with our experimental results. This circumstance does not require chemical stratification of the upper and lower mantle, supporting a compositionally homogenous mantle throughout the present-day mantle and whole-mantle

convection.

Variation of the transition width in the adiabatic mantle

Reference 26 suggested a potential expansion of the discontinuity thickness due to latent heat associated with a phase transition in an adiabatic mantle flow (Verhoogen effect) (Fig. 3), which was also reported by a geodynamic study[27]. The existing thermodynamic data suggest that the thickness of the present PSp transition could be expanded by ~7 km at most due to the latent heat of the PSp transition (See the Methods section). This expansion should lower reflectivity of short-wavelength *P*-wave at D660[28]. Reference 29 reported a decrease in short-wavelength *P*-wave reflectivity at D660 with approaching the mid-Atlantic ridge axis, which might be caused by possible vertical adiabatic flow under the ridge. Therefore, a global mapping of sharpness of D660 can be used to assess presence of vertical flows faster than thermal diffusion. The present study encourages global seismologists to revisit this topic to obtain new insights regarding mantle dynamics.

References

1. Xu, F., Vidale, J. E. & Earle, P. S. Survey of precursors to P′ P′: Fine structure of mantle discontinuities. *J. Geophys. Res. Solid Earth* **108** (2003).

2. Ito, E., Takahashi & E. Postspinel transformations in the system Mg_2SiO_4-Fe_2SiO_4 and some geophysical implications. *J. Geophys. Res. Solid Earth* **94**, 10637–10646 (1989).

3. Jackson, I. & Rigden, S. M. In The Earth's Mantle: Composition, Structure and Evolution (ed. Jackson, I.) 405–460 (Cambridge Univ. Press, 1998).

4. Irifune, T., Shinmei, T., McCammon, C. A., Miyajima, N., Rubie, D. C. & Frost, D. J. Iron partitioning and density changes of pyrolite in Earth's lower mantle. *Science* **327**, 193–195 (2010).

5. Hofmann, A. W. Mantle geochemistry: the message from oceanic volcanism. *Nature*, **385**, 219 (1997).

6. Schubert, G., Turcotte, D. L. & Olson, P. *Mantle Convection in the Earth and Planets*. (Cambridge University Press, 2001).

7. D. L. Anderson, *Theory of the Earth* (Blackwell Scientific, Boston, 1989).

8. Murakami, M., Ohishi, Y., Hirao, N. & Hirose, K. A perovskitic lower mantle inferred from high-pressure, high-temperature sound velocity data. *Nature* **485**, 90–94 (2012).

9. Nishiyama, N., Irifune, T., Inoue, T., Ando, J. I. & Funakoshi, K. I. Precise determination of phase relations in pyrolite across the 660km seismic discontinuity by in situ X-ray diffraction and quench experiments. *Phys. Earth Planet. Inter.* **143**, 185–199 (2004).

10. Katsura, T., Yamada, H., Shinmei, T., Kubo, A., Ono, S., Kanzaki, M., Yoneda, A., Walter, M. J., Ito, E., Urakawa, S., Funakoshi, K. & Utsumi W. Post-spinel transition in Mg_2SiO_4 determined by high P-T *in situ* X-ray diffractometry. *Phys. Earth Planet. Inter.* **136**, 11–24 (2003).

11. Akaogi, M., Kojitani, H., Matsuzaka, K., Suzuki, T. & Ito, E. "Postspinel transformations in the system Mg_2SiO_4–Fe_2SiO_4: element partitioning, calorimetry, and thermodynamic calculation" in *Properties of Earth and Planetary Materials at High Pressure and Temperature*. M. H. Manghnani, T. Yagi, Eds. (AGU, Washington, DC, 1998) vol. 101, pp. 373–384.

12. Ishii, T., Huang, R., Fei, H., Koemets, I., Liu, Z., Maeda, F., Yuan, L., Wang, L., Druzhbin, D., Yamamoto, T., Bhat, S., Farla, R., Kawazoe, T., Tsujino, N., Kulik, E., Higo, Y., Tange, Y. & Katsura, T. Complete agreement of the post-spinel transition with the 660-km seismic discontinuity. *Sci. Rep.* **8**, 6358 (2018).

13. Katsura, T., Yamada, H., Nishikawa, O., Song, M., Kubo, A., Shinmei, T., Yokoshi, S., Aizawa, Y., Yoshino, T., Walter, M. J. & Ito, E. Olivine-wadsleyite transition in the system $(Mg,Fe)_2SiO_4$. *J. Geophys. Res. Solid Earth* **109** (2004).

14. Fei, Y., Wang, Y. & Finger, L. W. Maximum solubility of FeO in (Mg, Fe)SiO_3-perovskite as a function of temperature at 26 GPa: Implication for FeO content in the lower mantle. *J. Geophys. Res. Solid Earth* **101**, 11525–11530 (1996).

15. Nakajima, Y., Frost, D. J. & Rubie, D. C. Ferrous iron partitioning between magnesium silicate perovskite and ferropericlase and the composition of perovskite in the Earth's lower mantle. *J. Geophys. Res. Solid Earth* **117** (2012).

16. Frost, D. J., Langenhorst, F. & Van Aken, P. A. Fe–Mg partitioning between ringwoodite and magnesiowüstite and the effect of pressure, temperature and oxygen fugacity. *Phys. Chem. Miner.* **28**, 455–470 (2001).

17. Frost, D. J. Fe^{2+}-Mg partitioning between garnet, magnesiowüstite, and $(Mg,Fe)_2SiO_4$ phases of the transition zone. *Am. Mineral.* **88**, 387–397 (2003).

18. Tange, Y., Nishihara, Y. & Tsuchiya, T. Unified analyses for P-V-T equation of state of MgO: A solution for pressure-scale problems in high P-T experiments. *J. Geophys. Res. Solid Earth* **114** (2009).

19. Fei, Y., Van Orman, J., Li, J., Van Westrenen, W., Sanloup, C., Minarik, W., Hirose, K., Komabayashi, T., Walter, W. & Funakoshi, K. Experimentally determined postspinel transformation boundary in Mg_2SiO_4 using MgO as an internal pressure standard and its geophysical implications. *J. Geophys. Res. Solid Earth* **109** (2004).

20. Holzapfel, C., Rubie, D. C., Mackwell, S., & Frost, D. J. Effect of pressure on Fe–Mg interdiffusion in (FexMg1− x) O, ferropericlase. *Phys. Earth Planet. Inter.*, **139**, 21-34 (2003).

21. Holzapfel, C., Rubie, D. C., Frost, D. J., & Langenhorst, F. Fe-Mg interdiffusion in (Mg, Fe)SiO$_3$ perovskite and lower mantle reequilibration. *Science*, **309**, 1707-1710 (2005).

22. Stixrude, L., & Lithgow-Bertelloni, C. Thermodynamics of mantle minerals-II. Phase equilibria. *Geophys. J. Int.*, **184**, 1180-1213 (2011).

23. Wood, B. J. Postspinel transformations and the width of the 670-km Discontinuity: A comment on "postspinel transformations in the system Mg$_2$SiO$_4$–Fe$_2$SiO$_4$ and some geophysical implications" by E. Ito and E. Takahashi. *J. Geophys. Res.: Solid Earth*, **95**, 12681-12685 (1990).

24. Katsura, T., Yoneda, A., Yamazaki, D., Yoshino, T. & Ito, E. Adiabatic temperature profile in the mantle. *Phys. Earth Planet. Inter.* **183**, 212–218 (2010).

25. Stixrude, L. Structure and sharpness of phase transitions and mantle discontinuities. *J. Geophys. Res.: Solid Earth*, **102**, 14835-14852 (1997).

26. Verhoogen, J. Phase changes and convection in the Earth's mantle. *Philos. Trans. R. Soc. London Ser.* **258**, 276–283 (1965).

27. Christensen, U. R. Dynamic phase boundary topography by latent heat effects. *Earth Planet. Sci. Lett.* **154**, 295-306 (1998).

28. Richards, P. G. Weakly coupled potentials for high-frequency elastic waves in continuously stratified media. *Bull. Seismol. Soc. Am.* **64**, 1575–1588 (1974).

29. Nakanishi, I. Reflections of P′ P′ from upper mantle discontinuities beneath the Mid-Atlantic Ridge. *Geophys. J.* **93**, 335–346 (1988).

Corresponding author

Takayuki Ishii (takayuki.ishii@uni-bayreuth.de)

Methods:

Preparation of starting materials

We used two starting materials with Mg_2SiO_4 (Fo_{100}) and $(Mg_{0.7}Fe_{0.3})_2SiO_4$ (Fo_{70}) bulk compositions. In order to examine the phase stability of Rw and Brg + fPc by normal (ringwoodite (Rw) → bridgmanite (Brg) + (ferro)periclase (f)Pc) and reversal (Brg + (f)Pc → Rw) reactions, these starting materials were prepared as fine mixtures with a grain size of 1–3 μm of Mg_2SiO_4 olivine (Ol) + $MgSiO_3$ enstatite (En) + reagent-grade MgO periclase (Pc) and $(Mg_{0.7}Fe_{0.3})_2SiO_4$ Ol + $(Mg_{0.9}Fe_{0.1})SiO_3$ En + $(Mg_{0.5}Fe_{0.5})O$ (fPc), respectively, with a molar ratio of 1:1:1. The Ol, En, and fPc were synthesized by the sol-gel method. Mg_2SiO_4 Ol and $MgSiO_3$ En synthesized by Ref. 12 were used. The fPc was synthesized from Mg and Fe metals, which were separately dissolved in HNO_3 with pure water. Tetraethylorthosilicate $((CH_3CH_2O)_4Si)$ was mixed with the solution in desired molar ratios of Mg:Fe:Si for Fe-bearing Ol and En. After ammonia was added in the solutions to make the gels, the gels were stepwisely heated up to 1700 K. Fe-bearing samples were heated at 1500 K for 12 h in a CO-CO_2 gas mix furnace controlled at an fO_2 of approximately 1 log unit above the iron-wüstite buffer. The pressure marker was prepared from reagent grade MgO with a grain size of 1 μm. The starting samples and the pressure marker were sintered for 1 h at 2 GPa and 800 K near Fe-FeO conditions (in the case of the Fe_{70} sample) made with a Mo foil capsule[30] using a Kawai-type multi-anvil press. The sintered samples were cut in the shape of disks with 1.2 mm in diameter and 0.5 mm thick, which were cut into half or quarter disks.

***In situ* X-ray diffraction experiments under high pressure and temperature**

High-pressure and high-temperature experiments combined with *in situ* X-ray measurement performed with the 15-MN Kawai-type multi-anvil press, SPEED-*Mk.*II, at the synchrotron radiation facility, SPring-8 (the beamline BL04B1)[31]. Tungsten carbide anvils (WC) (grade TF05 produced by Fuji Die Co. Ltd.) with a truncation of 4.0 mm were used to compress the samples. One-degree tapering was applied on anvil faces around a truncation, allowing a wide vertical opening for X-rays (0.7 mm at a maximum in this study) (Extended Data Fig. 2) and enhancing

high-pressure generation[32,33]. The cell assembly for *in situ* diffraction experiment is drawn in Extended Data Fig. 3. Pressure media were Cr_2O_3-doped semi-sintered MgO octahedra with a 10-mm edge length. The samples and the pressure marker with the shapes of quarter and half disks, respectively, were put at the center of the pressure media. The samples were surrounded by a 50-μm Mo foil, making the $Mo-MoO_2$ buffer conditions nearly equal to Fe-FeO as mentioned above. A $LaCrO_3$ cylindrical heater was set in a direction parallel to the incident X-rays. An MgO sleeve was put between the heater and Mo foil to insulate each other electrically. WC anvils and the heater were electrically connected by Ta electrodes. A ZrO_2 thermal insulator was positioned out of the heater. Both sides of the sample through the heater were filled by diamond/epoxy rods. Boron/epoxy rods were placed at both ends of the diamond/epoxy rods and in grooves of pyrophyllite gaskets along the X-ray path. Both rods played a role to suppress X-ray absorption in material. The diamond/epoxy rods with very low compressibility were also useful for keeping a wide opening for the X-rays in the heater under high P-T conditions. Temperatures were monitored using a $W_{97}Re_3-W_{75}Re_{25}$ thermocouple touching a surface of the Mo foil, which was inserted into the heater normal to the axis. The thermocouple was electrically insulated from the heater with alumina tubes. Temperature variations of a sample were measured in the direction parallel to an incident X-ray by Ref. 10. The variation within 20 K was estimated in the sample with 1-mm length in a parallel direction. Temperature variation in the present sample with the shorter sample length of 0.5 mm can be estimated to be less than 10 K because the present cell assembly was almost the same as in the previous study.

In situ energy-dispersive X-ray diffraction was conducted using white X-rays, which were typically collimated to 50 μm horizontally and 100–700 μm vertically with two variable incident slits. Diffracted X-rays at a 2θ angle of 7.2° were collected for 150–300 s using a germanium solid-state detector (SSD) in an energy range up to ca. 130 keV. Channel-energy relationships of the SSD were calibrated based on the energies of the X-ray emission line (Kα)

of [55]Fe and γ radiation from [57]Co and [133]Ba. Press-oscillation around the vertical axis between 0° and 7.2° were conducted in every X-ray diffraction measurement to suppress the problem from grain growth[31]. In order to calculate generated pressures, we used a volume change of MgO based on the third-order Birch-Murnaghan and Vinet equations of states (EOS) proposed by Ref. 18. In the calculation, the eight diffraction peaks (111, 200, 220, 311, 222, 400, 420, and 422) were typically used, rendering high precisions of ~0.05 GPa in pressure. Note that, in addition, high count-rates by the wide anvil opening for X-ray accommodation and "clean" diffraction patterns without additional peaks except for weak ones from diamond (Extended Data Fig. 1) are indispensable for obtaining such high precisions.

Experimental procedure in *in situ* X-ray diffraction experiments

Extended Data Figure 4a shows the typical change of *in situ* X-ray diffraction patterns of the Fo$_{70}$ sample (M2268). The samples were first compressed to a press load of 6–7 MN (28-29 GPa) at ambient temperature and then heated to 1100 K for 30–90 min to change the starting sample assemblage of Ol + En + (*f*)Pc to Rw + akimotoite (Ak) + (*f*)Pc [Extended Data Fig. 5a (I and II)]. This heating lowered a sample pressure to 22-23 GPa. While this temperature was being maintained, the sample pressure gradually decreased by ~1 GPa further spontaneously probably due to stress relaxation of the cell assembly and phase changes in the samples. Then, the press load was increased by 0.5–0.8 MN to reach a sample pressure of ~23 GPa, which is the target pressure at 1700 K [Extended Data Fig. 5a (III)]. The samples were then heated to 1700 K within 5 min. Just after reaching this temperature, the press load was immediately increased at a rate of ~0.05 MN/min for the first 5 min and then slowly at a rate of 0.01–0.02 MN/min to maintain sample pressures (forced pumping) [Extended Data Fig. 5a (IV)]. The increasing rate of press load was determined based on our experiences of the pressure variation while keeping temperature stable in preceding runs. Pressure variation and progress of the reaction in the samples were checked by collecting X-ray diffraction patterns of the pressure marker and samples

alternately while the temperature was kept constant. The samples were kept at the temperature for 0.5–2 h. They were then immediately cooled by cutting off the electric power supply to the heater and slowly returned to ambient conditions. Because the average temperature at the 660-km discontinuity is expected to be 2000 K[24], we also attempted experiments at 2000 K. However, we had extreme difficulty in keeping a target pressure constant at this temperature because of irreproducible pressure drop and lowering of pressure precision due to the disappearance of peaks of the MgO pressure marker caused by grain growth. For the above reasons, the experimental temperature of 1700 K for the present setup (Extended Data Figs. 2 and 3) was adopted.

Phase identification in *in situ* X-ray observation and analyses of recovered samples

In the Fo_{100} sample, Rw coexisted with a small amount of Brg + Pc below 23.8 GPa, whereas only Brg + Pc was present at higher pressures. The relatively fast and slow kinetics of the Ak-Brg transition[34,35] and formation of Rw from Brg plus Pc[10,36,37], respectively, suggest that the assemblage of Rw + Ak + Pc formed at 1100 K should have first transformed to Rw + Brg + Pc during increasing temperature, and then the majority of Brg and Pc was consumed to form more Rw in the Rw stability field. Therefore, we conducted not only the normal run (Rw => Brg + Pc) but also the reversal run (Brg + Pc => Rw) using the same starting material in each run. We interpreted that the runs with the mineral assemblage of Rw + Brg + Pc were results of Rw stability. The coexistence of Brg + Pc was because each of their grains is isolated by Rw grains, as already reported by Ref. 12 (Extended Data Figure 4). Since Brg and Pc were stable in each system (i.e. bridgmanite in the $MgSiO_3$ system and periclase in the MgO system) at our investigated pressure range (23-25 GPa)[19,38], the complete reversal reaction was hampered due to this separation. On the other hand, no Rw was found in the stability field of Brg + Pc due to destabilization of Rw above the transition pressure and its fast kinetics[10].

In the Fo_{70} sample, the assemblages of Brg + fPc + St and Rw + fPc + St were observed above and below 23.76 GPa, respectively. In contrast to the Fo_{100} sample, no Brg was observed at lower

pressures. The absence of Brg was due to decomposition of Brg to the Rw + St with Fe-rich compositions[39].

Micro-textures of starting and recovered samples were observed using a field-emission-type scanning electron microscope (Zeiss LEO 1530 Gemini) with an energy dispersive X-ray spectrometer (Oxford X-Max$^{\mathrm{N}}$). Phases present in the starting and recovered samples were confirmed with a laboratory micro-focused X-ray diffractometer (Brucker AXS Discover 8). We had difficulty in determining compositions of phases in the recovered samples because each grain in the recovered samples was too small to conduct electron microprobe analysis and Rw grains contain inclusions of *f*Pc and St due to fine-grain mixing in the starting materials. We therefore estimated an Mg-Fe partition coefficient between Mg endmember and the boundary of four-phase coexistence by the following thermodynamic calculation. We also emphasize that it is unlikely that equilibrium compositions are obtained at this temperature due to inertness of Brg[15].

Estimation of the widths of the post-spinel transition binary loops at 1700 and 2000K in (Mg$_{0.9}$Fe$_{0.1}$)$_2$SiO$_4$

Compositions of Brg and Rw for a given *f*Pc composition were calculated by Mg-Fe partitioning between Brg and *f*Pc and between Rw and *f*Pc as follows. Note that no Fe^{3+} is assumed in this calculation because of reduced conditions produced by the Mo tubes and diamond/Epoxy rods.

The Mg-Fe exchange equilibrium between Brg and *f*Pc can be written as

$$\mathrm{MgSiO_3^{Brg} + FeO^{\mathit{f}Pc} = FeSiO_3^{Brg} + MgO^{\mathit{f}Pc}} \quad (1)$$
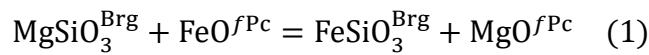
The free energy change of pure components, $\Delta_{\mathrm{Brg\text{-}fPc}}G^0_{P,T}$ for Eq. (1) can be written as

$$\Delta_{\mathrm{Brg-fPc}}G^0_{P,T} = -RT\ln\frac{a_{\mathrm{Fe}}^{\mathrm{Brg}}a_{\mathrm{Mg}}^{\mathrm{fPc}}}{a_{\mathrm{Mg}}^{\mathrm{Brg}}a_{\mathrm{Fe}}^{\mathrm{fPc}}} \quad (2)$$

where a_i^A is the activity of the *i* component in phase *A*. The activity is expressed as

$$a_i^{\mathrm{A}} = X_i^{\mathrm{A}} \cdot \gamma_i^{\mathrm{A}} \quad (3)$$

where X_i^A and γ_i^A are mole fraction and activity coefficient of *i* component in phase *A*, respectively.

$X_{Fe}{}^{A}$ is described as

$$X_{Fe}^{A} = \left(\frac{Fe^{2+}}{Fe^{2+} + Mg^{2+}}\right) \quad (4)$$

The partition coefficient $K_D{}^{Brg\text{-}fPc}$ for this reaction is defined as

$$K_D^{Brg-fPc} = \frac{X_{Fe}^{Brg} X_{Mg}^{fPc}}{X_{Mg}^{Brg} X_{Fe}^{fPc}} \quad (5)$$

Using Eqs. (3) and (5), Eq. (2) can be rewritten as

$$\Delta_{Brg-fPc}G_{P,T}^{0} = -RT\ln K_D^{Brg-fPc} - RT\ln\frac{\gamma_{Fe}^{Brg}\gamma_{Mg}^{fPc}}{\gamma_{Mg}^{Brg}\gamma_{Fe}^{fPc}} \quad (6)$$

Here, we assume that both solid solutions are regular symmetric solutions, which allows writing activity coefficients for each solid solution as

$$RT\ln\gamma_i^{A} = W_{Mg\text{-}Fe}^{A}\left(1 - X_i^{A}\right)^2 \quad (7)$$

where $W^{A}{}_{Mg\text{-}Fe}$ is a symmetric interaction parameter of component i in phase A.

By substituting Eq. (7) into Eq. (6) and rearranging, we obtain the following equation:

$$RT\ln K_D^{Brg-fPc} = -\Delta_{Brg-fPc}G_{P,T}^{0} - W_{Mg\text{-}Fe}^{Brg}\left(1 - X_{Fe}^{Brg}\right)^2 - W_{Mg\text{-}Fe}^{fPc}\left(1 - X_{Mg}^{fPc}\right)^2$$
$$+ W_{Mg\text{-}Fe}^{Brg}\left(1 - X_{Mg}^{Brg}\right)^2 + W_{Mg\text{-}Fe}^{fPc}\left(1 - X_{Fe}^{fPc}\right)^2 \quad (8)$$

Similarly, the Mg-Fe exchange equilibriums between Rw and fPc can be expressed as

$$MgSi_{0.5}O_2^{Rw} + FeO^{fPc} = FeSi_{0.5}O_2^{Rw} + MgO^{fPc} \quad (9)$$
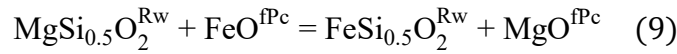
In the same way as the Mg-Fe exchange equilibriums between Brg and fPc, we have

$$RT\ln K_D^{Rw-fPc} = -\Delta_{Rw-fPc}G_{P,T}^{0} - W_{Mg\text{-}Fe}^{Rw}\left(1 - X_{Fe}^{Rw}\right)^2 - W_{Mg\text{-}Fe}^{fPc}\left(1 - X_{Mg}^{fPc}\right)^2$$
$$+ W_{Mg\text{-}Fe}^{Brg}\left(1 - X_{Mg}^{Rw}\right)^2 + W_{Mg\text{-}Fe}^{fPc}\left(1 - X_{Fe}^{fPc}\right)^2 \quad (10)$$

The compositions of Brg and Rw for a given fPc composition are obtained using the partition coefficients given by Eq. (8) and (10), respectively. The necessary thermochemical parameters in Eq. (8) and (7) are given in Extended Data Table 2.

To depict a binary loop of the PSp transition, equilibrium of Mg and Fe components

should be considered as follows:

$$Mg_2SiO_4^{Rw} = MgSiO_3^{Brg} + MgO^{fPc} \quad (11)$$

$$Fe_2SiO_4^{Rw} = FeSiO_3^{Brg} + FeO^{fPc} \quad (12)$$
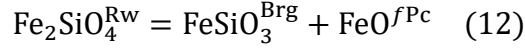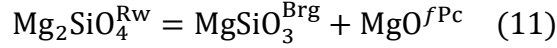
In usual ways, equilibrium compositions and transition pressures should be obtained by equality of chemical potentials between the right and left sides of Eq. (11) and (12). However, it is found that consistent results between Eqs. (11) and (12) based on the partition coefficients given by Eq. (8) and (10) are not obtained. This is certainly due to lack of reliable thermochemical parameters, especially of Fe endmember of bridgmanite. In this study, therefore, the binary loop is depicted by estimating the pressures that three phases with compositions estimated from the partition coefficients coexist, which are evaluated using the equation of the Mg components (Eq. (11)).

The Gibbs energy change for Eq. (11) is given as

$$\Delta_{PSp\ tr.}G_{P,T}^0 = \Delta_{PSp\ tr.}H_T^0 - \Delta_{PSp\ tr.}S_T^0 + \int_{1\ atm}^{P} \Delta_{PSp\ tr.}V_{P,T}^{Mg} + RT\ln\frac{a_{Mg}^{Brg}a_{Mg}^{fPc}}{\left(a_{Mg}^{PSp}\right)^2} = 0 \quad (13)$$

$\Delta_{PSp\ tr.}H_T^0$, $\Delta_{PSp\ tr.}S_T^0$ and $\Delta_{PSp\ tr.}V_{P,T}^{Mg}$ are enthalpy, entropy and volume changes for Eq. (11), respectively. For the Mg-endmember, activities of the phases are equal to unity in Eq. (13), namely

$$\Delta_{PSp\ tr.}G_{P,T}^0 = \Delta_{PSp\ tr.}H_T^0 - \Delta_{PSp\ tr.}S_T^0 + \int_{1\ atm}^{P_{Mg}} \Delta_{PSp\ tr.}V_{P,T}^{Mg} + RT\ln 1 = 0 \quad (14)$$

where P_{Mg} is the PSp transition pressure of the Mg endmember.

By substituting Eq. (14) into Eq. (13) and assuming that $\Delta_{PSp\ tr.}V_{P,T}^{Mg}$ is constant due to the very narrow experimental pressure interval, we have

$$(P - P_{Mg})\Delta_{PSp\ tr.}V_{P,T}^{Mg} + RT\ln\frac{a_{Mg}^{Brg}a_{Mg}^{fPc}}{\left(a_{Mg}^{PSp}\right)^2} = 0 \quad (15)$$

Using Eqs. (3) and (7), Eq. (15) can be written as

$$(P - P_{Mg})\Delta_{\text{PSp tr.}}V_{P,T}^{Mg} = RT\ln\frac{X_{\text{Mg}}^{\text{Brg}}X_{\text{Mg}}^{\text{fPc}}}{\left(X_{\text{Mg}}^{\text{PSp}}\right)^2} - W_{\text{Mg-Fe}}^{\text{Brg}}\left(1 - X_{\text{Mg}}^{\text{Brg}}\right)^2 - W_{\text{Mg-Fe}}^{\text{fPc}}\left(1 - X_{\text{Mg}}^{\text{fPc}}\right)^2$$

$$+2W_{\text{Mg-Fe}}^{Rw}\left(1 - X_{\text{Mg}}^{Rw}\right)^2 \tag{16}$$

Equation (16) gives a pressure by inputting equilibrium compositions of the three phases. It is noted that the compositional width of the binary loop at each pressure is assured by the Mg-Fe partitioning among the three phases.

We started this calculation from $X_{\text{Mg}}^{\text{fPc}} = 0.002$ and increased $X_{\text{Mg}}^{\text{fPc}}$ by 0.002 step by step. The compositions of the other two phases and pressure were calculated at each step. Reference 14 reported that the maximum $FeSiO_3$ solubility in bridgmanite is 0.093 at 1700 K. The calculation was terminated when $X_{\text{Mg}}^{\text{Brg}}$ reached this value. It is noted that Ref. 14 claimed that they conducted their experiments at a pressure of 26 GPa. However, we consider that they overestimated their pressure values because (1) they calibrated sample pressure only at ambient temperature, (2) they extrapolated the pressure values from data points below 22.5 GPa. Since it is unknown at what pressure they conducted their runs, we assume that their pressure should have been also 24 GPa.

The errors in these calculations were evaluated from the errors in published thermochemical data, which are also shown in Extended Data Table 2, based on the law of propagation of errors. We estimated the pressure intervals at a bulk composition of $(Mg_{0.9}Fe_{0.1})_2SiO_4$ and temperatures of 1700 and 2000 K to be 0.012 ± 0.008 and 0.003 ± 0.002 GPa, respectively.

Effect of geotherm on discontinuity thickness

If the geotherm is nearly isothermal around the phase boundary (G_1 in Fig. 3), the PSp transition occurs over a narrow interval of D_1. However, if the geotherm is adiabatic, temperatures in the Rw region should be higher than in the Brg + fPc region because of the endothermicity of the PSp transition. As a result, the geotherm in the Rw and Brg + fPc regions intersects at points a

and b, and therefore, the PSp transition occurs over an interval of D_4, which is called the Verhoogen effect. If the flow is very slow, and the temperature profile is diffused as the geotherm G_2 and G_3 in Fig. 3, the interval D_2 and D_3 will be between D_1 and D_4[40].

Estimation of thickness increment due to the Verhoogen effect

Latent heat (ΔT_{LH}) by the PSp transition of Rw with Fo$_{90}$ was calculated as below. If a phase transition occurs at adiabatic conditions, the geotherm is deflected along an equilibrium phase boundary because of latent heat associated with the phase transition. The temperature change by the latent heat (ΔT_{LH}) is calculated from

$$\Delta T_{LH} = \frac{T \Delta V (dP/dT)}{\overline{C_P}} \quad (17)$$

where T is temperature, ΔV ($[V_{Mg}^{Brg} \times X_{Mg}^{Brg} + V_{Fe}^{Brg} \times (1-X_{Mg}^{Brg})^{Brg}] + [V_{Mg}^{/Pc} \times X_{Mg}^{/Pc} + V_{Fe}^{/Pc} \times (1-X_{Mg}^{/Pc})] - [V_{Mg}^{Rw} \times X_{Mg}^{Rw} + V_{Fe}^{Rw} \times (1-X_{Mg}^{Rw})]$) the change in volume across the transition, dP/dT the Clapeyron slope of the transition, and $\overline{C_P}$ the average isobaric heat capacity (e.g. Ref. 41).

Thermochemical and thermoelastic data of each phase used in the calculation are summarized in Extended Data Table 3. The Clapeyron slope of the PSp transition was considered to be between −3 MPa/K and −1 MPa/K (e.g., Refs 2, 10, 19, 42). P and T were 23.4 GPa and 2000 K, respectively. Our calculation shows the ΔT_{LH} was 30-90 K, leading to the thickness increment due to the Verhoogen effect being 0.03-0.27 GPa. Thus, we obtained the maximum thickness increase of 6.7 km.

Data availability

Details of the cell assembly used, representative X-ray diffraction patterns, a back-scattered electron image of Mg$_2$SiO$_4$ recovered sample, parameters for the thermodynamic calculations, and supplementary discussion of thermodynamic calculations to discuss effects of secondary components can be seen in the supplementary information. Any additional data can be requested

by emailing the corresponding author Takayuki Ishii at takayuki.ishii@uni-bayreuth.de.

Methods references

30. Xu, Y., McCammon, C. & Poe, B. T. The effect of alumina on the electrical conductivity of silicate perovskite. *Science* **282**, 922–924 (1998).

31. Katsura, T., Funakoshi, K. I., Kubo, A., Nishiyama, N., Tange, Y., Sueda, Y. I., Kubo, T. & Utsumi, W. A large-volume high-pressure and high-temperature apparatus for *in situ* X-ray observation, 'SPEED-Mk. II'. *Phys. Earth Planet. Inter.* **143**, 497–506 (2004).

32. Ishii, T., Shi, L., Huang, R., Tsujino, N., Druzhbin, D., Myhill, R., Li, Y., Wang, L., Yamamoto, T., Miyajima, N., Kawazoe, T., Nishiyama, N., Higo, Y., Tange, Y. & Katsura, T. Generation of pressures over 40 GPa using Kawai-type multi-anvil press with tungsten carbide anvils. *Rev. Sci. Instrum.* **87**, 024501 (2016).

33. Ishii, T., Yamazaki, D., Tsujino, N., Xu, F., Kawazoe, T., Liu, Z., Yamamoto, T., Druzhbin, D., Wang, L., Higo, Y., Tange, Y., Yoshino, T. & Katsura, T. Pressure generation to 65 GPa in a Kawai-type multi-anvil apparatus with tungsten carbide anvils. *High press. Res.* **37**, 507–515 (2017).

34. Kuroda, K. *et al.* Determination of the phase boundary between ilmenite and perovskite in MgSiO$_3$ by in situ X-ray diffraction and quench experiments. *Phys. Chem. Miner.* **27**, 523–532 (2000).

35. Ono, S., *et al.* In situ observation of ilmenite–perovskite phase transition in MgSiO$_3$ using synchrotron radiation. *Geophys. Res. Lett.* **28**, 835–838 (2001).

36. Irifune, T. *et al.* The postspinel phase boundary in Mg$_2$SiO$_4$ determined by *in situ* X-ray diffraction. *Science* **279**, 1698–1700 (1998).

37. Shimojuku, A., Boujibar, A., Yamazaki, D., Yoshino, T., Tomioka, N. & Xu, J. Growth of ringwoodite reaction rims from $MgSiO_3$ perovskite and periclase at 22.5 GPa and 1,800° C. *Phys. Chem. Miner.* **41**, 555–567 (2014).

38. Ishii, T., Kojitani, H. & Akaogi, M. Post-spinel transitions in pyrolite and Mg_2SiO_4 and akimotoite–perovskite transition in $MgSiO_3$: precise comparison by high-pressure high-temperature experiments with multi-sample cell technique. *Earth Planet. Sci. Lett.* **309**, 185–197 (2011).

39. Ito, E. & Yamada, H. "Stability relations of silicate spinels, ilmenites, and perovskites" in *High-pressure research in geophysics*, S. Akimoto, M. H. Manghnani, Eds. (Center for Academic Publishing Japan, Tokyo, 1982) vol. 12, pp 405–419.

40. Schubert, G., Turcotte, D. L., & Olson, P. Mantle convection in the Earth and planets (Cambridge University Press, Cambridge, UK, 2001).

41. Bina, C. R. A note on latent heat release from disequilibrium phase transformations and deep seismogenesis. *Earth planet. Space* **50**, 1029-1034 (1998).

42. Kojitani, H., Inoue, T. & Akaogi, M. Precise measurements of enthalpy of postspinel transition in Mg_2SiO_4 and application to the phase boundary calculation. *J. Geophys. Res. Solid Earth* **121**, 729–742 (2016).

Author contributions

T.I. conducted the majority of the experiments, analyzed all the samples and data, conducted thermodynamic analysis in the Mg_2SiO_4–Fe_2SiO_4 system and wrote the manuscript. T. Katsura directed this project. R.H. and T. Katsura conducted trial runs of preliminary experiments. R.H. and H.F. helped in starting sample preparations. I.K. helped to establish the cell assembly. R.M. conducted thermodynamic calculations to discuss effects of secondary components. F.M., L.Y., Z.L., L.W., D.D., T.Y., S.B., R.F., T. Kawazoe, T.N., E.K., Y.H., and Y.T. operated synchrotron radiation experiments at the beamline BL04B1 at SPring-8. All authors discussed the results and commented on the manuscript.

Competing Interests: The authors declare that they have no competing interests.

Figure captions

Figure 1. **Phase relations in the system Mg_2SiO_4-Fe_2SiO_4.** X_{Mg} is the Mg/(Mg+Fe) ratio.

Compositions of three phases (Rw, Brg, and fPc) were shown by solid line. Dashed lines are a rough-drawing of phase boundaries in this system. (a) The phase relations at 1700 K. Open and solid circles indicate that stable phases are Rw and Brg + Pc, respectively. Open and solid triangles indicate that stable phases are Rw + fPc + St and Brg + fPc + St, respectively. (b) Estimated shift of the phase boundaries from 1700 (blue) to 2000 K (red).

Figure 2. **Back-scattered electron images of the samples recovered from 23.86 GPa and 1700 K (M2268).** (a) The whole image of the sample. (b) Magnified image of the $(Mg_{0.7}Fe_{0.3})_2SiO_4$ sample. The gray, white, and black grains are ringwoodite, ferropericlase, and stishovite respectively, indicating the stability of the ringwoodite-bearing assemblage (c) Magnified image of the Mg_2SiO_4 sample. The white and gray grains are bridgmanite and periclase, respectively, indicating the stability of the post-spinel phases. TC: thermocouple; P.M.: MgO pressure marker; Brg: bridgmanite; Pc: periclase; Rw: ringwoodite; fP: ferropericlase; St: stishovite.

Figure 3. **Expansion of discontinuity thickness of the post-spinel transition boundary by the Verhoogen effect[26].** Isothermal geotherm is shown by G_1 (dashed line), making the transition thickness of D_1 (0.25 km). Black solid line is the phase boundary of the post-spinel transition. Complete adiabatic geotherm is shown by G_4 (yellow solid line), forming D_4 (7 km at most) due to latent heat (30-90 K). If the geotherm is under intermediate conditions (G_2, G_3 dashed curves), the latent-heat effect should be smeared and give D660 thickness between D_1 and D_4 (D_2, D_3) depending on flow direction.